# A Novel Method of High Accuracy, Wavefront Phase and Amplitude Correction for Coronagraphy

Charles W. Bowers[a], Bruce E. Woodgate[a], Richard G. Lyon[b]
[a]Goddard Space Flight Center, Code 681, Greenbelt, Maryland, USA 20771
[b]Goddard Space Flight Center, Code 930, Greenbelt, Maryland, USA 20771

## ABSTRACT

Detection of extra-solar, and especially terrestrial-like planets, using coronagraphy requires an extremely high level of wavefront correction. For example, the study of Woodruff et al. (2002) has shown that phase uniformity of order $10^{-4}\lambda$(rms) must be achieved over the critical range of spatial frequencies to produce the $\sim 10^{10}$ contrast needed for the Terrestrial Planet Finder (TPF) mission. Correction of wavefront phase errors to this level may be accomplished by using a very high precision deformable mirror (DM). However, not only phase but also amplitude uniformity of the same scale ($\sim 10^{-4}$) and over the same spatial frequency range must be simultaneously obtained to remove all residual speckle in the image plane. We present a design for producing simultaneous wavefront phase and amplitude uniformity to high levels from an input wavefront of lower quality. The design uses a dual Michelson interferometer arrangement incorporating two DM and a single, fixed mirror (all at pupils) and two beamsplitters: one with unequal (asymmetric) beam splitting and one with symmetric beam splitting. This design allows high precision correction of both phase and amplitude using DM with relatively coarse steps and permits a simple correction algorithm.

**Keywords:** coronagraphy

## 1. INTRODUCTION

Discovery of numerous exo-planets by radial velocity measurements combined with significant technological advances make the direct imagery and spectroscopy of such planets a foreseeable possibility. Instrumentally, two different space-borne approaches for exo-planet imagery have received much attention, namely interferometry and coronagraphy. In this paper we will deal only with the coronagraphic approach. Observationally there are roughly two classes of objects: Jovian size planets and terrestrial size planets, distinguished by the contrast suppression of their parent stars necessary to produce stellar stray light ~ planetary flux (i.e. Q~1). For Jovian-like systems a stellar suppression of $\sim 10^{-9}$ at angular scales of ~4-100$\lambda$/D while for terrestrial-like planets, suppression of $\sim 10^{-10}$ at similar angular scales is necessary.

Suppression of optical diffraction to such a high level is theoretically possible for optically perfect systems using various coronagraphic systems several of which have been compared in detail[1]. However deviations of wavefront phase uniformity at very low levels (commonly referred to as scatter) will introduce "speckle" in the focal plane, a distribution of light which reflects the spatial frequency distribution of phase errors in the pupil. Speckle light can effectively overwhelm a faint planetary image and is not suppressed by a classical coronagraph. In their study of various approaches for a TPF coronagraph, Woodruff et al.[1], conclude that, over the critical range of spatial frequencies, a phase uniformity of ~50pm or ~$\lambda$/12,000 at 600nm is required to reduce speckle to an acceptable level.

This degree of wavefront correction has never been achieved in a large scale space-borne telescope. The most studied means of achieving the necessary phase uniformity is through the use actuators on the primary mirror to control low spatial frequency phase errors supplemented by a deformable mirror (DM) placed in the optical train prior to the coronagraph to correct mid-frequency spatial errors. DM technology and control systems are becoming more mature; Trauger et al.[2] have demonstrated an excellent power spectral density (PSD) result with a Xinetics DM equivalent to an rms surface error of 0.03nm over the spatial frequency range needed for a Jovian-like planet detection mission.

Not as widely appreciated is the fact that wavefront amplitude must also be corrected to comparable levels as phase uniformity or the result will again be focal plane speckle. The requirement of very high amplitude uniformity over a range of aperture frequencies is new for telescope opticians. The level to which amplitude uniformity can be attained during manufacture and passively maintained through a complex optical system is largely unknown at the present.

With these considerations in mind, we have begun to look at various means of providing simultaneous active correction of both phase and amplitude to the levels required for TPF. In this paper we investigate some means of producing such correction using the well developed DM technology.

## 2. EFFECTS OF NON-UNIFORM AMPLITUDE ON CORONAGRAPHY

The effect of small levels of pupil amplitude non-uniformity in imaging is similar to phase non-uniformity, namely creation of "speckles" in the image. The field in the image plane is the Fourier transform of the pupil function $Ae^{i\phi}$ with amplitude A and phase $\phi$. For small aberrations the Fourier transform takes the form

$$F(Ae^{i\phi}) \Rightarrow A_0F(1 + \frac{\delta A}{A_0} + i\delta\phi) = A_0F(1 + \frac{\delta A}{A_0} + 2\pi i\delta\phi_\lambda)$$

where $\delta\phi_\lambda$ is the phase error in waves and we have retained only first order terms in the aberrations, $\frac{\delta A}{A_0}$ and $\delta\phi$ The form of the aberrations in the focal plane is the same (except for a $\frac{\pi}{2}$ phase shift). Thus where Woodruff et al.[1] show that phase errors of ~λ/12,000 are the limit to produce contrast of ~$10^{-10}$ with a Lyot coronagraph suitable for TPF, we would expect amplitude errors of about $5x10^{-4}$ to provide a similar limit for amplitude non-uniformities for the same conditions.

To more accurately determine the effect of amplitude non-uniformities for coronagraphy, we have simulated the effects of a series of amplitude aberrated pupils when used with a Lyot coronagraph. The results are summarized in Figure 1. The image intensity profile of a centrally located star is plotted for various levels of amplitude non-uniformity (rms). For a specific level of rms amplitude error, an image was calculated showing the expected speckle pattern. At each radial distance the contrast (image intensity over a resolution element compared to the total, central star intensity) was determined and the median value of the intensity distribution at each radius has been plotted as a single point. Smoothed versions of these results are shown as solid lines.

A distribution of amplitude errors were chosen with varying rms amplitude. In all cases, the amplitude PSD was set to have a power law frequency dependence with index -2. Frequencies of 1-64 cycles/aperture were included. The coronagraph was a Lyot type with a focal plane stop having a radial Gaussian transmission function with the half-transmission point at 4λ/D. The Lyot stop was 0.72 of the beam radius.

From the figure we can get approximate levels of allowable amplitude non-uniformity for the two interesting cases of $10^{-9}$ and $10^{-10}$ contrast, corresponding to Jovian and terrestrial exo-planet detection requirements. Beyond 4λ/D distances, ~$10^{-9}$ contrast can be achieved for amplitude non-uniformity of about 0.0018 (intensity ~0.0036); ~$10^{-10}$ contrast is achievable for amplitude non-uniformity levels less than about 0.0005 (intensity ~0.001). We note that in any real system both amplitude and phase errors will be present and contribute to the loss of contrast. However these results indicate the high level of amplitude uniformity that must be achieved in addition to phase uniformity in order to produce sufficient contrast for exo-solar planet detection.

The requirement of very high amplitude uniformity over a particular band of spatial frequencies is not a typical consideration for astronomical instruments and there is little information on the quality of current technology regarding this requirement. Simple calculations of ideal coatings on a fast, primary mirror for example, indicate that variations of a few $10^{-4}$ may be expected, with power concentrated in the lower spatial frequencies, accompanied by a comparable level of polarization (we do not deal with polarization effects in this work, though its effects will also be important to consider for TPF). Any real observatory will have multiple components as well, each adding to the overall system amplitude non-uniformity. Amplitude uniformity may be much more stable than phase (figure) uniformity which can easily be changed by thermal changes. However, for the long term, the creation of pinholes and effects of contamination at the very low levels required for TPF make the question of amplitude stability over observatory lifetimealso problematic .

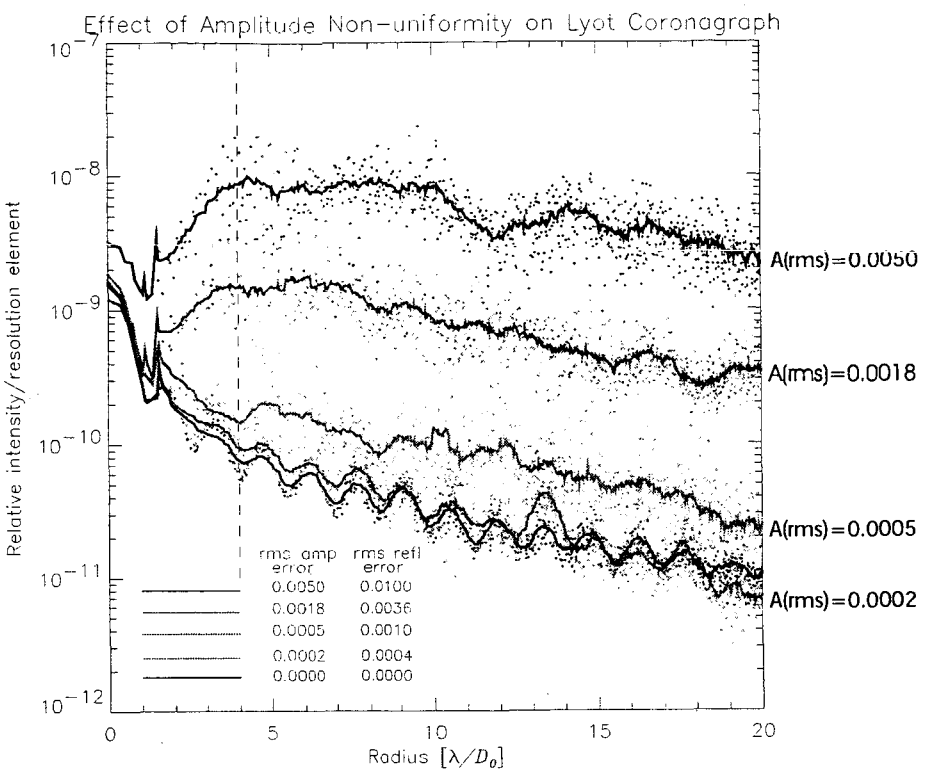


Figure 1: Simulation results of various rms levels of amplitude non-uniformities (indicated by labels to right of each curve for A(rms)≠0) on the contrast achievable with a Lyot coronagraph. Zero phase error is assumed for each simulation. The amplitudes follow a $f^{-2}$ power law distribution with the indicated rms level errors. The Lyot coronagraph has a focal plane Gaussian profile transmission stop with half maximum transmission at 4λ/D and a hard, Lyot stop of radius 0.72. Contrast levels of ~$10^{-9}$ can be achieved with an amplitude rms of about 0.0018 (intensity of about 0.0036) and contrast of $10^{-10}$ can be achieved with rms non-uniformity of about 0.0005 amplitude (intensity of 0.001).

## 3. ASYMMETRIC DUAL MICHELSON CONFIGURATION

Since it appears that active correction of both amplitude and phase will be required for TPF, we will consider a means to simultaneously correct both parameters. We suppose a wavefront corrector assembly which will take the input, aberrated wavefront from the telescope, correct phase and amplitude errors and pass on this highly corrected wavefront to the coronagraph. Current TPF coronagraphic designs (Woodruff et al.[1] for example) have a similar assembly but provide a means of phase correction only. Two questions which must be answered for such a corrector is what specific device will be used for correction and at what point in the optical path should such devices be situated (focal plane, pupil plane or somewhere between)?

Littman et al.[3] have proposed using two pixellated spatial light modulators (SLM) to provide such correction, point by point across the beam. The SLM are used in a zero-path-difference Michelson interferometer configuration with each replacing the usual rigid mirrors in each interferometer arm. Because the technology of deformable mirrors (DM) is currently more advanced than spatial light modulators and has some other clear advantages (mirror coatings can be largely achromatic, with low scatter for example) we have instead chosen to explore the possible use of multiple DM to provide correction of both phase and amplitude. In principle, two DM located in the optical path provide enough degrees of freedom to correct the wavefront in both phase and amplitude even though they are intrinsically pure phase

altering devices. These devices could be positioned at conjugate pupils, replacing the rigid mirrors of a zero-path-difference Michelson interferometer as suggested by Littman et al[3] using SLM. Such a configuration has the advantage of relatively easy derivation of the system properties and can capitalize on the extensive development of DM already made[2].

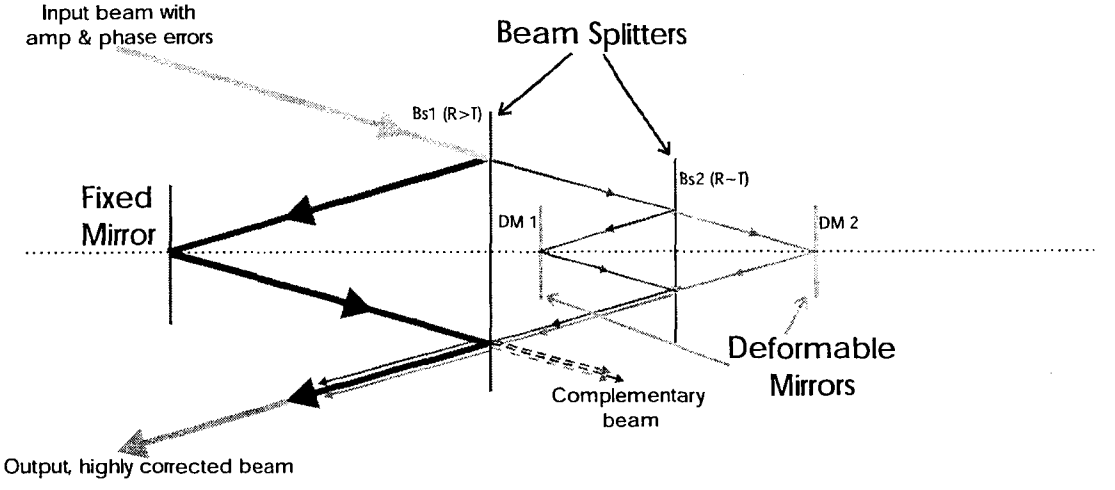


Figure 2: A schematic layout of the dual asymmetric Michelson corrector. The input, aberrated beam is asymmetrically split by the first beamsplitter (BS1) which reflects most light to a fixed mirror and into the output beam unchanged. The light transmitted through BS1 is symmetrically split at BS2 into two beams, each directed toward a deformable mirror. The figure of each DM is adjusted, point-by-point across the beam, altering the phases at each point of the beams. All three beams are recombined forming a highly corrected beam at the output. A small amount of light is also present in the complementary beam and may be useful for active monitoring of wavefront quality during observations.

A modification of the simple Michelson design, which we have termed the asymmetric dual Michelson configuration is shown in Figure 2. In this design, we assume that the aberrated wavefront is of relatively good quality but still several orders of magnitude from the $\sim 10^{-4}$ level needed for TPF. In this case, we should need relatively minor, but highly precise, modification of the wavefront to produce the necessary correction. This is done by (see Figure 2) providing an asymmetric beamsplitter (BS1) which reflects most of the beam from input to output via a rigid, stationary mirror. A relatively small amount of light is transmitted through the beamsplitter to the correction section; the initial reflected beam and that from the correction section comprise a Michelson interferometer. Within the corrector section itself we once again beam split, this time in an equal division, forming a second, nested Michelson interferometer arrangement. Following appropriate adjustment of the two DM, this faint correction beam is recombined with the stronger, aberrated and reflected beam to produce a combined beam which is highly corrected. The major advantage of such a configuration is that it permits very precise adjustments of amplitude and phase with DM capable of only lower precision. This also makes such a configuration more stable to drift of the DM figure over the length of an observation since the overall precision can be much less dependent on DM accuracy (see Section 4.1). We have chosen, in this study, to use only two DM, the minimum number which provide the necessary degrees of freedom for phase and amplitude correction and so keep the system as simple as possible for a space borne mission.

The correction method of such a configuration can be illustrated with a simple phasor diagram representing the three complex fields from the single rigid and two adjustable DM at the point where the fields are combined (Figure 3). We represent the amplitude and phase from each of the three field components at a single point in the beam as three vectors with length equivalent to field amplitude and phase angle represented by the orientation of the vectors with respect to the real axis. This analysis is monochromatic; the chromatic properties are addressed in Section 6. If we can adjust the DM, point-by-point across the beam so that the combined field has the same amplitude and phase everywhere in the beam, then the wavefront has been perfectly corrected. We have freedom to adjust the relative amplitudes of the fields by selecting the reflectance and transmission of the beamsplitters, though once selected the same relative field amplitudes

are set for all points in the beam. For each point in the beam we can adjust the field phases for the two DM beams but have no control over the field phase from the rigid mirror beam.

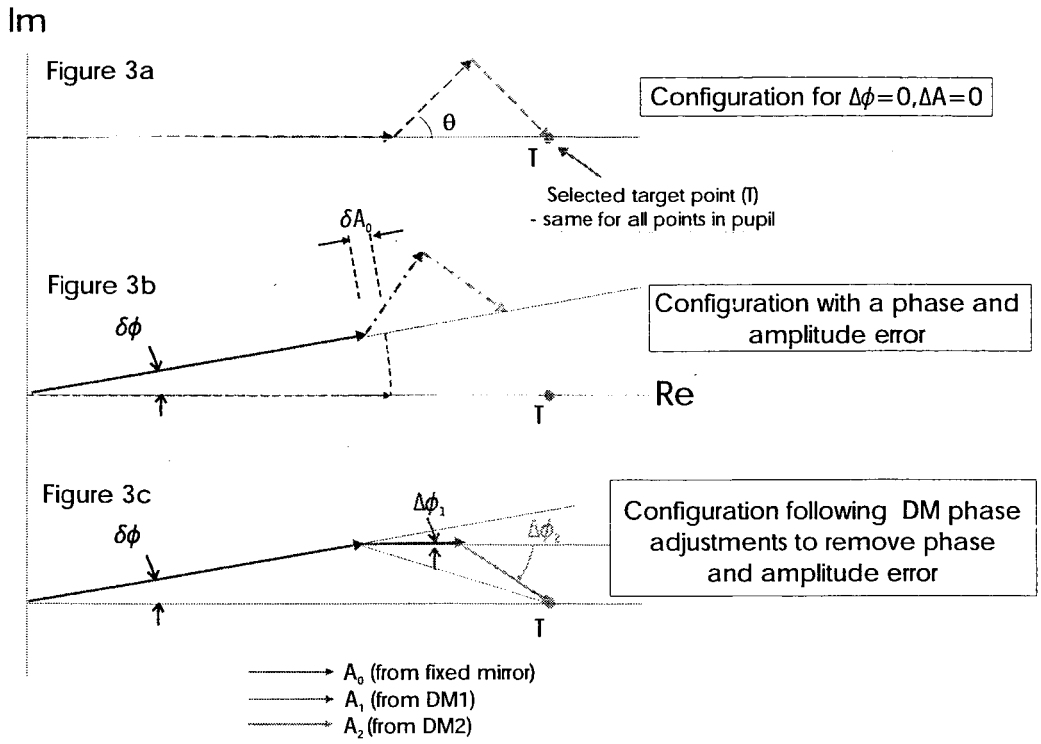


Figure 3: The upper panel (3a) illustrates the field configuration for an asymmetric dual Michelson with no phase or amplitude errors. The DM have equal and opposite steps (phase shifts). The target point is selected so that the total field amplitude is just less than all amplitudes in the beam. Figure 3b (middle panel) shows how the field components are altered if a phase and amplitude error is introuduced at this point in the beam. All three fields have equal phase shifts (rotation) and proportionally reduced amplitudes. The lower panel (figure 3c) illustrates the means of correction of the aberrations shown in the central panel. The field component due to the rigid mirror cannot be changed but the two DM are adjusted by altering their local height, inducing phase changes which make the total field terminate at the target point, just as the unaberrated configuration shown in the top panel.

For the case of no phase and amplitude error we arrange the DM phases as shown in Figure 3a. In this case the field component from the rigid mirror has it's full amplitude and zero phase error. We then select a target point T with zero phase error and an amplitude ≤ to the weakest field amplitude across the beam. The phase (rotation) of the two DM is adjusted so the combined vector terminates at the target point. For zero phase and amplitude error (Figure 3a) this means deflecting the two DM by equal and opposite amounts, or in phase space, rotating the vectors representing fields from the DM through equal and opposite angles.

For points in the beam which similarly have no phase error but do have reduced amplitude, we have a configuration like that of Figure 3a except, as the field amplitudes decrease, we deflect the DM less (less vector rotation) so the combined beam still terminates at the same target point. Figures 3b and 3c show the more general case of both an amplitude and phase error compared to the unaberrated case (Figure 3a). The phase error is represented by a rotation of all three field vectors and a reduction of amplitude shortens the length of all three vectors proportionally. While there is no adjustment possible for the strong field component from the rigid mirror, we can still adjust the phases (rotations) of the two DM reflected components to produce a combined field which again terminates on the target point. The fields following adjustment are illustrated in Figure 3c.

Examination of these figures indicates several important aspects of the asymmetric Michelson configuration with DM for phase adjustment. First, the amplitude relationship between the DM reflected fields and the rigid mirror reflected field (set by the initial selection of beamsplitter properties) combined with our inability to control the phase of the rigid mirror field component, means that we will have a limited phase range over which we produce phase correction. Correction over the full range of amplitude variations can be assured by selecting the target point amplitude sufficiently small. However the smaller the target point amplitude the less light is in the beam passed through to the coronagraph (intensity $\propto$ amplitude$^2$) and the greater is the intensity of the complementary beam (see Figure 2). For our simulations (Section 5) we have assumed the target amplitude to be 0.93 giving an overall transmission of 0.86. (This amplitude range is much greater than would likely occur in a real system but was selected to illustrate the significant range which can be corrected.) Finally, we note that the case of a single Michelson configuration can be considered as a variant of the asymmetric dual design where the field amplitude from the rigid mirror goes to zero. This single Michelson arrangement has advantages in some cases which we will examine.

## 4. ACCURACY OF CORRECTION AND CAPTURE RANGE

### 4.1 Accuracy of correction

The change of combined field phase and amplitude ($\Delta\Phi$,$\Delta A$) with a phase change of one DM device is easy to derive for the case of zero phase error. Figure 4 illustrates the geometry for this situation. From the figure, it is clear that relatively large phase steps at the DM can result in fine adjustment of the combined field amplitude and phase, through the relative difference between the amplitudes from the rigid mirror ($A_0$) and the DM ($A_1$) effected by the asymmetric beamsplitter.

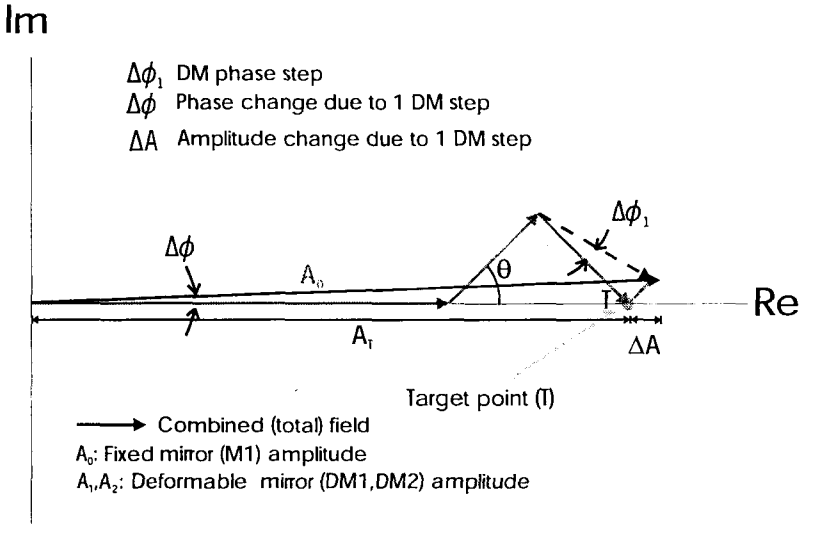


Figure 4: The change of amplitude and phase of the combined field due to the phase change of a single DM is illustrated. Because of the different amplitudes, $A_0$ and $A_1$, between the beams from the rigid and DM mirrors respectively, a relatively coarse phase change of the DM ($\Delta\phi_1$) results in smaller changes ($\Delta A$,$\Delta\phi$) in the combined field amplitude and phase.

The relationships between these quantities can be derived with the following results. The change in combined field phase is -

$$\tan(\Delta\phi) = \frac{(\frac{A_1}{A_0})\Delta\phi_1 \cos\theta}{1+2(\frac{A_1}{A_0})\cos\theta}$$

and the change in amplitude is -

$$\frac{\Delta A}{A_T} = \frac{(\frac{A_1}{A_0})\Delta\phi_1 \sin\theta}{1+2(\frac{A_1}{A_0})\cos\theta}$$

These relationships can be simplified for the cases of the asymmetric dual Michelson with $\frac{A_1}{A_0} \ll 1$and the single Michelson with $\frac{A_1}{A_0} \gg 1$ and are summarized in Table 1.

Table 1: Correction Accuracy

| | Asymmetric Dual Michelson $\frac{A_1}{A_0} \ll 1$ | Single Michelson $\frac{A_1}{A_0} \gg 1$ |
|---|---|---|
| $\Delta\phi_T$ [waves] | $\frac{\Delta\phi_1}{2\pi}(\frac{A_1}{A})\cos\theta$ | $\frac{1}{2}(\frac{\Delta\phi_1}{2\pi})$ |
| $\frac{\Delta A_T}{A}$ | $\Delta\phi_1(\frac{A_1}{A})\sin\theta$ | $\frac{1}{2}\Delta\phi_1 \tan\theta$ |

The advantage of the asymmetric, dual Michelson in terms of resolution in both amplitude and phase is clear from the proportionality to the relative amplitudes of the DM (A1) and the rigid mirror (A0). For $A_1/A_0$ small, a relatively coarse DM step ($\Delta\phi_1$) can still produce very precise amplitude and phase correction of the combined field. For the single Michelson, this multiplier is fixed at the value ½, but this can be much smaller for an asymmetric system. We also note that a single DM phase step produces both phase and amplitude changes in the combined field and that the relative distribution of the changes depends on the initial DM phase angle $\theta$, which is set to accommodate the range of amplitude which must be corrected.

**4.2 Range of correction**

The range of phase error which can be corrected using an asymmetric dual Michelson configuration is illustrated in Figure 5. The amplitudes between the beams from the rigid mirror ($A_0$) and the two DM ($A_1$, $A_2$; in the following we assume $A_1$=$A_2$) are determined by the choice of reflectance and transmittance of the two beamsplitters. The DM phase angle ($\theta$) is selected to permit correction of the range of amplitude non-uniformities. The limit of phase correction is reached when the two DM fields are configured, with the same offset phase, as shown by the dashed line in Figure 5. Any greater phase error $\phi$ (producing an increased rotation of the rigid mirror field) results in a combined field which cannot terminate at the target point for any combination of DM phase adjustments. Also note that since this maximum correctable phase depends on the relative amplitudes of the rigid and DM fields, a decrease in field amplitudes will result in a decrease of the correctable phase range.

The relation between the amplitudes, initial phase orientation $\theta$ and the maximum correctable phase angle can be determined to be

$$\cos\phi = 1 - \frac{2(\frac{A_1}{A_0})^2 \sin^2\theta}{1+2(\frac{A_1}{A_0})\cos\theta}$$

The reduction in correctable phase range with decreasing amplitudes, referred to above, is reflected in this expression by the decrease in angle $\theta$ as the amplitudes decline.

We can simplify this relation for the case of highly asymmetric dual Michelson $(\frac{A_1}{A_0} \ll 1)$as

$$\cos\phi \sim 1 - 2(\frac{A_1}{A_0})^2 \sin^2\theta$$

$$\phi \sim \pm 2(\frac{A_1}{A_0})\sin\theta \text{ [rad]} = \pm(\frac{A_1}{A_0})(\frac{\sin\theta}{\pi}) \text{ [waves]}$$

As a specific example, suppose $A_1 = 0.1A_0$ . Then the range of possible phase correction is $\leq \pm 0.032$ waves. The exact value will depend on the target point chosen (determining the initial offset phase angle $\theta$) which depends on the required range of amplitude correction.

We note that for the single Michelson configuration ($A_0 = 0$), we don't have such a range restriction though, as discussed above, the requirements for DM accuracy are greater.

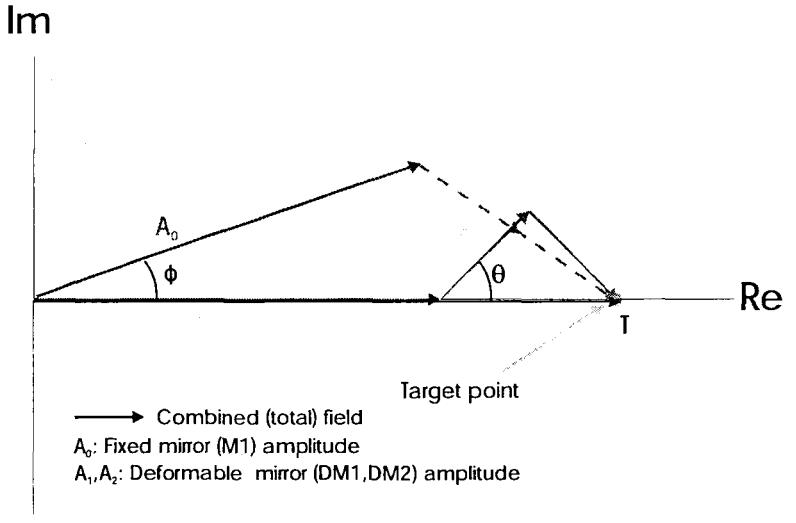


Figure 5: The range of phase correction for the asymmetric dual Michelson configuration is illustrated. The original, zero phase error configuration is shown by the solid lines. As the wavefront phase error increases, the phase of the field from the rigid mirror ($A_0$) rotates. The DM phases are adjusted so the combined field still terminates at the target point T. As the phase error continues to increase, the DM are eventually adjusted as shown with the dashed lines. Any further increase of phase error will make DM adjustment of phase unable to produce a field which terminates at T and the correction will be incomplete.

## 5. TWO SAMPLE DESIGNS

In this section we consider two example corrector designs: a single Michelson design to pre-TPF (Jovian-like planet imager) requirements and a dual asymmetric Michelson design to TPF (terrestrial-like planet imager) requirements. The results shown are based on simulations using specified distributions of phase and amplitude errors. For both parameters we assumed PSD with $1/f^2$ dependence, and a frequency bandwidth of 1-64 cycles/aperture. Correction was made using the same simple algorithm in both cases, illustrated in Figure 3c. For these simulations, correction was made at all points in the generated field ($386^2$ pixels). The effects of more limited DM actuator density and the effects of the actuator influence function have not been included; these will be device specific and should be part of a more complete simulation. We also have assumed in these simulations no errors in wavefront sensing of the fields from the fixed and DM mirrors; we assume that we are able to accurately measure the amplitude and phase of the fields from the three mirrors. Insertion of shutters in the beam paths shown in Figure 2 and measurement at the field combination region (after passage through the corrector) would permit such measurements of each field component in turn. The corrector designs have specific limitations on the correction range of phase and amplitude as discussed in Section 4. For a distribution of random field errors as described by the PSD with a specified rms error level, cases in which the amplitude or phase exceeds the correctable range can occur. In these cases, where phase adjustment of the two DM could not fully correct the wavefront, we oriented the DM (set their respective step heights) to produce a combined field which is as close as possible to the selected target point. All these simulations were monochromatic. We illustrate the wavefront correction of the corrector itself and the resulting contrast when such a wavefront is injected into the same Lyot coronagraph model detailed in Section 2.

### 5.1 pre-TPF corrector

This corrector is designed for pre-TPF requirements, namely to achieve contrast of about $10^{-9}$ in order to image Jovian-like exoplanets. We select a single Michelson design for its ability to correct over phase error of a full wave and it's simplicity, both qualities which make it attractive for relatively near term use. The single Michelson configuration requires higher accuracy in the DM adjustment than the asymmetric dual Michelson. However since the contrast requirements are not as great in this example as for TPF, we can still relax the tolerance on the DM step accuracy and achieve the necessary contrast.

Table 2 contains the values of the relevant design parameters used in this simulation. We set the initial phase angle of the two DM to 21.6 degrees yielding a very large range of amplitude correction (±3.5%). With phase control over both mirrors (no fixed mirror present in this system), the phase correction range is a full wave. The target point amplitude was selected to be 0.93 yielding a high intensity transmission of 0.86. The remaining 0.14 intensity will appear in the complementary beam (see Figure 2) and may be used for monitoring wavefront quality during an exposure.

Table 2: Single Michelson Corrector System Parameters

| | |
|---|---|
| DM step size | 1/400λ (1.5nm@λ=600nm) |
| Beamsplitters | |
| BS1 | absent |
| BS2 | R/T=0.5/0.5 |
| Field amplitudes | A0=0, A1=A2=0.5 |
| Target point | |
| amplitude | 0.93 (transmission =0.86) |
| phase | 0.0 |
| Correction range limits | |
| phase | ±0.5λ |
| amplitude | ±0.035 |

Table 3: Wavefront Error Distribution Characteristics

| | |
|---|---|
| Uncorrected Wavefront | |
| PSD | $\propto 1/f^2$ |
| bandwidth | 1-64 cycles/aperture |
| Phase errors | |
| rms | $3.0\times10^{-2}$ λ |
| range | $\pm1.2\times10^{-1}\lambda$ |
| Amplitude errors | |
| rms | $7.0\times10^{-3}$ |
| range | $\pm2.9\times10^{-2}$ |
| Corrected Wavefront | |
| Phase errors | |
| rms | $1.0\times10^{-3}\lambda$ |
| range | $\pm2.5\times10^{-3}$ λ |
| Amplitude errors | |
| rms | $1.7\times10^{-3}$ |
| range | $\pm5.0\times10^{-3}$ |

Figure 6 illustrates the results of the corrector using images which represent the distribution of wavefront error (phase and amplitude) before and following correction. The phase error has been reduced from $3\times10^{-2}$ λ rms to $1\times10^{-3}$ λ rms and the amplitude error reduced from $7\times10^{-3}$ rms to $1.7\times10^{-3}$ rms.

Figure 7 illustrates the magnitude of the correction and the distribution of residual errors through plots of the distribution of phase and amplitude errors before and following correction. The substantial improvement in both phase and amplitude errors is evident. Also evident is the correlation between the residual errors following correction, indicated by the diamond shaped distribution of Figure 7b. Since each DM adjustment changes both phase and amplitude it is not surprising that the residuals will be correlated.

Figure 8 shows the improvement in performance of the model Lyot coronagraph with the corrected wavefront. Contrast has improved by 4-5 orders of magnitude by correction and the pre-TPF goal of contrast ~$10^{-9}$ or less beyond 4λ/D has been achieved.

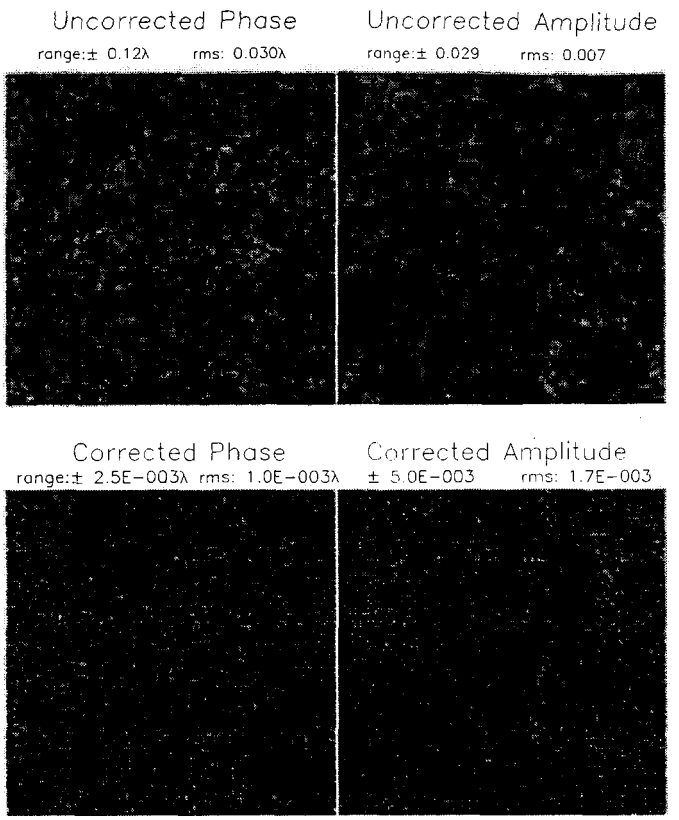


*Figure 6*: Images of the wavefront errors before (upper panels) and following (lower panels) correction using the single Michelson with two deformable mirrors. The left panels show phase error, the right show amplitude error. The values above each panel indicate the range (maximum and minimum values in the error distribution) and rms of the particular error distributions.

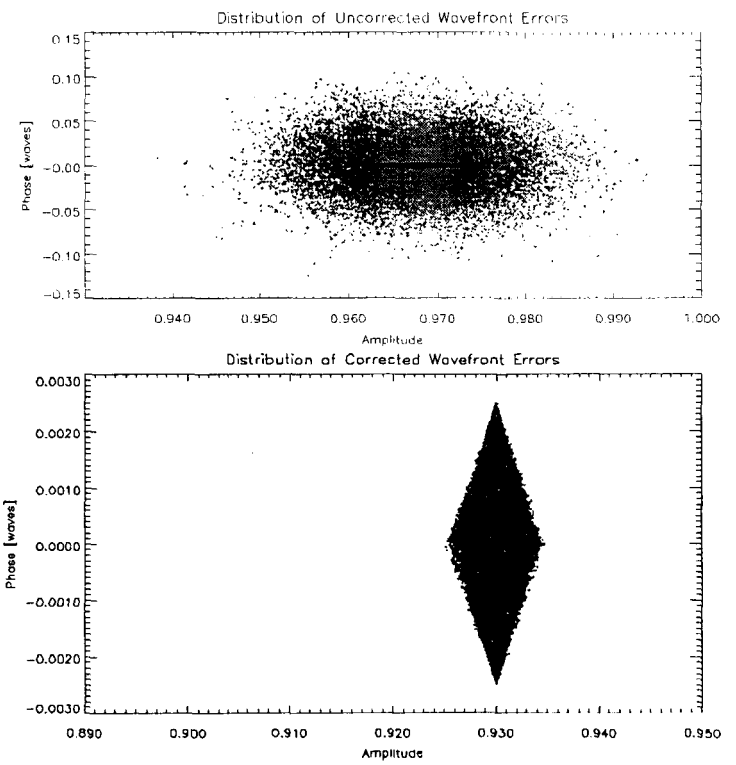


Figure 7: Plots showing the distribution of amplitude and phase errors before (upper panel) and following (lower panel) correction with the single Michelson configuration. Note that the scales of the panels are significantly different. The correlation between amplitude and phase in the residual errors following correction is evident from the diamond shaped error pattern of the lower panel.

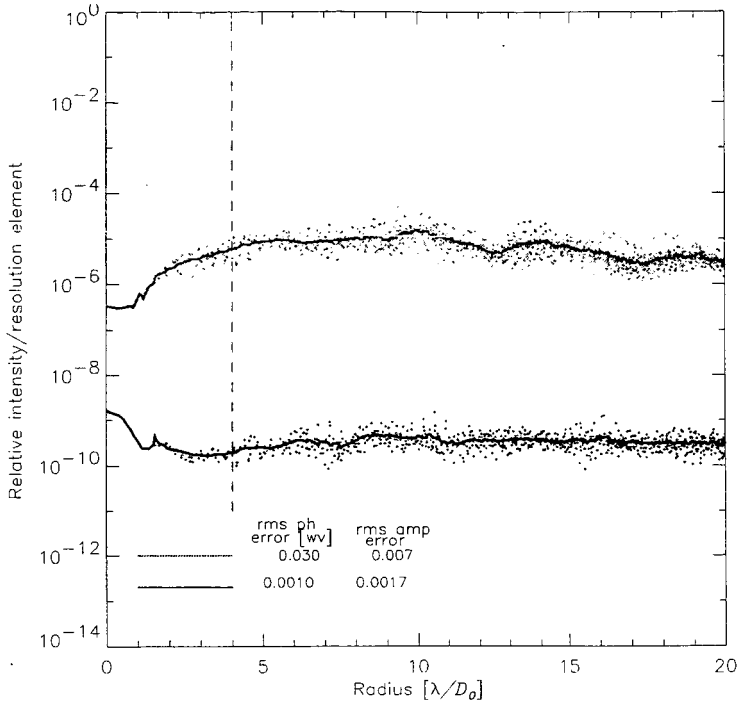


Figure 8: Profiles of the coronagraphic output PSF without (upper curve) and with (lower curve) correction using the single Michelson corrector. The relative intensity/resolution element has been corrected by 4-5 orders of magnitude and now achieves the $10^{-9}$ level necessary for Jovian-like exo-planet imagery.

### 5.2 TPF corrector

This corrector is designed for the more demanding TPF requirements. We assume that the telescope and ancillary optics are corrected to a somewhat higher degree than in the pre-TPF case; the corrector will again reduce the wavefront error this time to achieve ~$10^{-10}$ contrast to enable imagery of terrestrial-like exoplanets. In this case we use an asymmetric dual Michelson design. We selected an initial 50:50 beamsplitter, sending equal light to the rigid mirror and the two DM. This ratio was selected to maintain a large phase correction range (±0.060λ). This imposes a greater requirement on DM accuracy (1/1200λ); if the input wavefront can be improved more, a proportional reduction in DM step precision is possible.

Table 4 contains the values of the relevant parameters used in this simulation. The initial phase angle of the two DM was set to 30.7 degrees yielding the same very large range of amplitude correction (±3.5%) as in the pre-TPF example. Also, as in that example, the target point amplitude was selected to be 0.93 yielding a high intensity transmission of 0.86. The uncorrected amplitude distribution has an rms of 0.5% compared to the design full range of correction of 3.5%. The design range of phase correction (±0.060λ) is about 4 times the rms phase distribution of uncorrected errors.

Figure 9 illustrates the results of the corrector using images which represent the distribution of wavefront error (phase and amplitude) before and following correction. The phase error has been reduced from $1.4\text{x}10^{-2}\lambda$ rms to $1.6\text{x}10^{-4}\lambda$ rms and the amplitude error reduced from $5\text{x}10^{-3}$ rms to $4.6\text{x}10^{-4}$ rms.

Figure 10 illustrates the distribution of phase and amplitude errors before and following correction. Note that the two panels have very different scales. The substantial improvement in both phase and amplitude is very evident. In the lower panel (error distribution following correction) a few points are plotted which have errors in excess (all with lower amplitude) of the main distribution of residual errors. These are due to points which had a combination of initial phase and amplitude error which put them just beyond the correctable phase range and so were only partially corrected. The number of these is small and they will have a negligible effect on coronagraphic performance.

Table 4: Dual Asymmetric Michelson Corrector System Parameters

| | |
|---|---|
| DM step size | 1/1200λ (0.5nm@λ=600nm) |
| Beamsplitters | |
| BS1 | R/T=0.5/0.5 |
| BS2 | R/T=0.5/0.5 |
| Field amplitudes | A0=0.5, A1=A2=0.25 |
| Target point | |
| amplitude | 0.93 (transmission =0.86) |
| phase | 0.0 |
| Correction range limits | |
| phase | ±0.060λ |
| amplitude | ±0.035 |

Table 5: Wavefront Error Distribution Characteristics

| | |
|---|---|
| Uncorrected Wavefront | |
| PSD | $\propto 1/f^2$ |
| bandwidth | 1-64 cycles/aperture |
| Phase errors | |
| rms | $1.4 \times 10^{-2}\lambda$ |
| range | $\pm 5.6 \times 10^{-2}\lambda$ |
| Amplitude errors | |
| rms | $5.0 \times 10^{-3}$ |
| range | $\pm 1.9 \times 10^{-2}$ |
| Corrected Wavefront | |
| Phase errors | |
| rms | $1.6 \times 10^{-4}\lambda$ |
| range | $\pm 7.1 \times 10^{-4}\ \lambda$ |
| Amplitude errors | |
| rms | $4.6 \times 10^{-4}$ |
| range | $\pm 6.1 \times 10^{-3}$ |

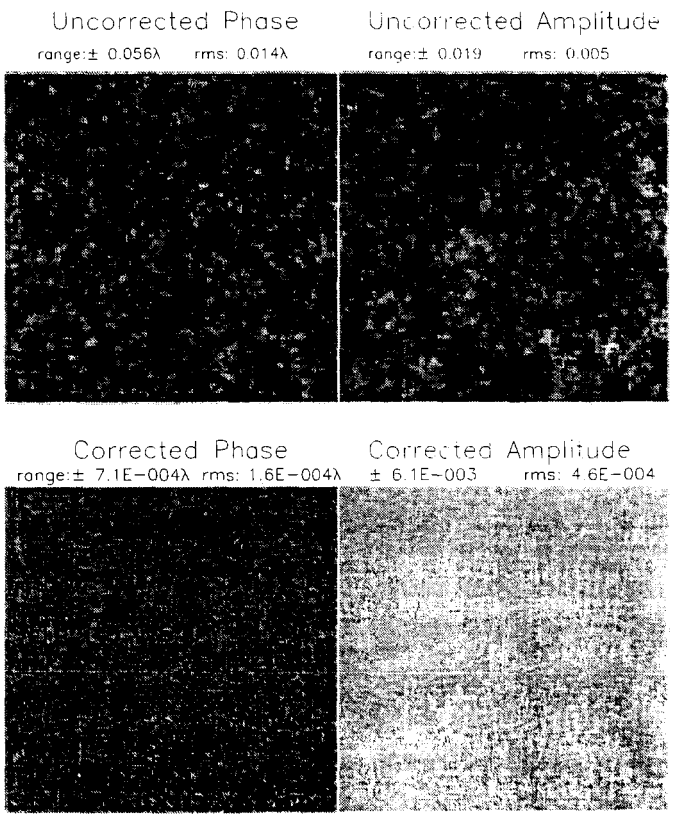


Figure 9: Images of the wavefront errors before (upper panels) and following (lower panels) correction using an asymmetric dual Michelson with two deformable mirrors. The left panels show phase error, the right show amplitude error. The values above each panel indicate the range (maximum and minimum values in the error distribution) and rms of the particular error distributions.

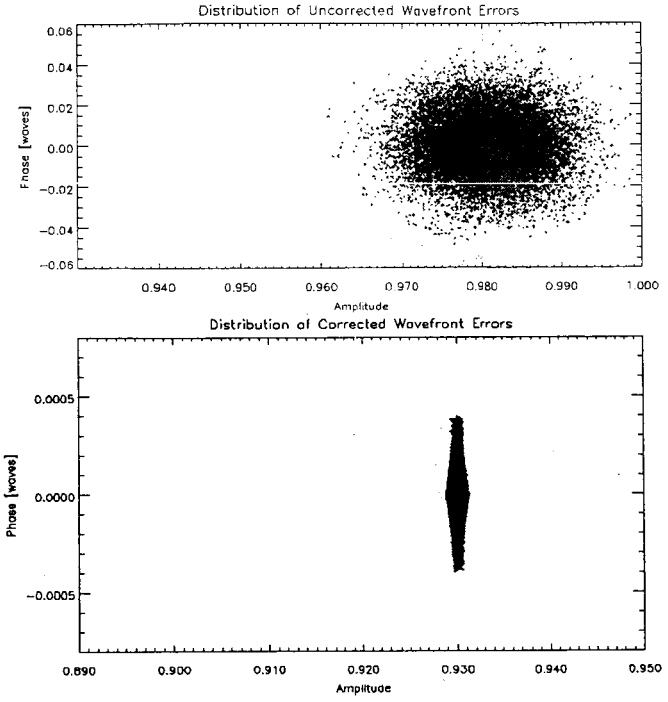


Figure 10: Plots showing the distribution of amplitude and phase errors before (upper panel) and following (lower panel) correction with asymmetric dual Michelson configuration. Note that the scales of the panels are significantly different. The outlier points in the corrected distribution are due to a few points in the uncorrected error distribution which exceeded the phase range limit for this design and so had less than nominal correction.

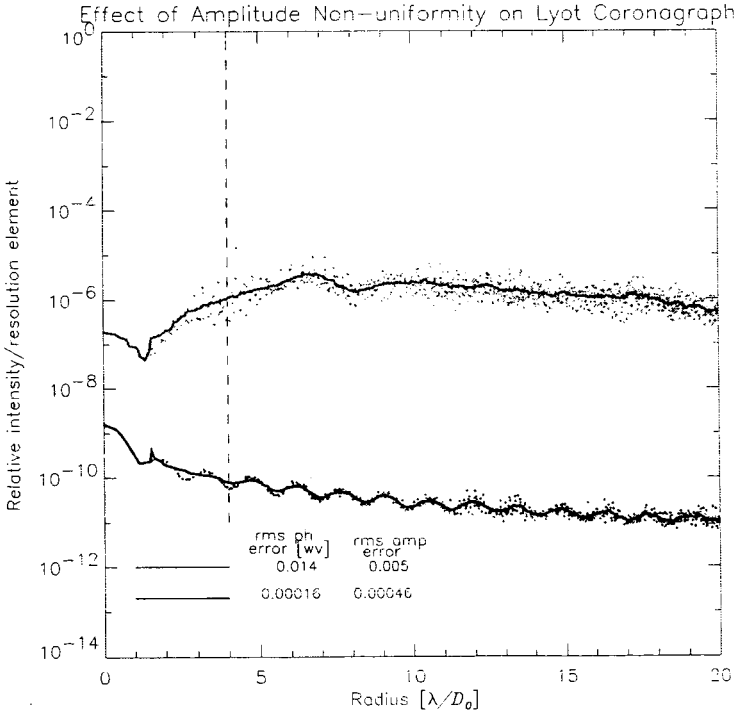


Figure 11: Profiles of the coronagraphic output PSF without (upper curve) and with (lower curve) correction using the asymmetric dual Michelson system. The relative intensity/resolution element has been corrected by 4-5 orders of magnitude and now achieves the $10^{-10}$ level necessary for terrestrial exo-planet imagery.

Figure 11 shows the effect of the uncorrected and corrected wavefront when used as input to the Lyot coronagraph model detailed in section 2. The contrast has improved 4-5 orders of magnitude from just over $10^{-6}$ to $\leq 10^{-10}$ at radii greater than $4\lambda/D$, meeting the TPF requirement. At this level of correction there is no significant difference between this wavefront and a perfect wavefront as far as contrast with the Lyot coronagraph.

## 6. CHROMATIC PROPERTIES

In these designs, the DM mirrors (and rigid mirror in the case of the dual asymmetric Michelson) are at conjugate pupils and all results have been calculated for monochromatic light. The effect of broad band light can be seen by reference to Figure 3a, showing the dual asymmetric Michelson fields in a zero phase error configuration. The two DM have equal and opposite step heights (d) to keep the total phase zero but reduce the amplitude slightly so that a range of amplitude errors can also be corrected. Suppose this is the configuration for the shortest wavelength of a bandpass $\Delta\lambda$. As the wavelength increases, the relative phase differences due to the fixed DM step height, d, decreases. The two phasors representing the fields from the DM in Figure 3a, rotate toward the real axis and the total field amplitude increases. The total field phase stays at zero; the effect of the finite bandpass is to cause an effective amplitude error (increase) of the total field with greater wavelength. We can derive some expressions for the magnitude of the finite bandpass amplitude error for this simple case to get an idea of the acceptable bandpass for the dual asymmetric (and also the single ) Michelson designs.

The total length of the two DM fields along the real axis is

$$s = 2A_1 \cos\theta$$

For a small change in phase angle $\theta$, due here to the change of wavelength, the change in this length (corresponding to a change in amplitude) is

$$\Delta A = 2A_1 \Delta\theta \sin\theta$$

The change in phase angle with a change in wavelength can be expressed as

$$\theta = \frac{2\pi}{\lambda}(2d)$$

$$\partial\theta = \frac{2\pi(2d)}{\lambda^2} d\lambda = \theta\frac{\partial\lambda}{\lambda}$$

$$\Delta\theta = \frac{\theta}{R}$$

Where $R = \frac{\lambda}{\partial\lambda}$, is the ratio of the nominal wavelength to the bandpass, a term known as resolving power in spectroscopy. Combining these gives a relation for the change of amplitude with wavelength, $\Delta A_\lambda$ as

$$\Delta A_\lambda = 2A_1 \sin\theta \left(\frac{\theta}{R}\right)$$

The amplitude error is minimal for small $A_1$ (highly asymmetric configuration), narrow bandpass (large R) and especially for a small initial DM phase angle $\theta$.

However, is is also useful to consider the range of amplitude correction, $A_C$ , for a given configuration of $A_1$, and $\theta$.

$$A_C = (2A_1 + A_0) - (s + A_0) \approx 2A_1(1 - \cos\theta)$$

A small value of initial DM phase angle $\theta$, which provides the least bandpass error, also produces the least range of amplitude correction. Thus there is a trade between the required amplitude correction range and the effective bandpass over which amplitude errors are negligible.

These two conditions can be combined as

$$R\Delta A_\lambda = A_C\theta\left(\frac{\sin\theta}{1-\cos\theta}\right)$$
$$\Rightarrow 2A_C \mid_{\theta\to 0}$$

This gives a relation between the bandpass (through resolving power R), the amplitude error due to finite bandpass ($A_\lambda$) and the range of amplitude correction ($A_C$). This result applies to either the single or asymmetric dual Michelson

configuration.

As a specific example, assume we allow the bandpass error to equal $5x10^{-4}$, approximately the minimum value of amplitude error for TPF requirements. In this case, if the necessary amplitude correction range is 0.5% (this is the total correction range - the distribution of amplitude errors should have an rms a few times smaller to make sure nearly all points are fully corrected), then a value of R=20 is determined. That is, the allowable bandpass is 1/20 of the nominal wavelength.

## 7. SUMMARY

We have proposed and performed some initial analysis of an interferometric wavefront corrector which could be used with a coronagraph for high contrast imaging particularly for a pre-TPF or TPF mission. The corrector uses two DM placed at conjugate pupils. The purpose of this device is to provide both phase and amplitude correction to a wavefront to the very high levels necessary for exo-solar planetary imagery, and we have illustrated the effects of amplitude non-uniformity, in particular, with a Lyot coronagraph model. The asymmetric dual Michelson has the advantage of achieving high precision correction with less accurate DM devices and is less sensitive to DM drift during observations. It does have a limited phase correction range but this may be satisfactory for the optical quality to be used in these missions. A single Michelson can correct a full wave of phase error but has higher requirements on DM accuracy and stability. Example designs using both variations have been provided and simulated and show that they can produce the required phase and amplitude uniformity levels. An estimate of the allowable bandpass has also been provided.

## REFERENCES


1. Woodruff, R., Ridgeway, S., Lyon, R., Burrows, C. , Gezari, D., Harwit, M., Melnick, G., Nisenson, P., Spergel, D.,Kaylor, L., Peterson, L., Friedman, E., Kaplan, M., "Feasibility of and Technology Roadmap for Coronagraphic Approaches to TPF",NASA NRA 01-OSS-04, Extra-Solar Planets Advanced Mission Concepts, Type 3 Study, 2002.
2. J. T. Trauger, D. Moody, B. Gordon, Y. Gürsel, M. A. Ealey, R.B. Bagwell, "Performance of a precision high-density deformable mirror for extrememly high contrast imaging astronomy from space", *Future EUV/UV and Visible Space Astrophysics Mission and Instrumentation*, ed. J. Chris Blades and Oswald H. W. Siegmund, 4854, p. 1-8, SPIE, Bellingham, WA, 2002.
3. M.G. Littman, M. Carr, J. Kasdin, R. Vanderbei, D. Spergel, "Amplitude Control: Closing the Loop", American Astronomical Society Meeting 201, poster 19.03, Jan 2003.